UNIVERSITY OF AMSTERDAM

UvA-DARE (Digital Academic Repository)

Spectroscopic Study of a Cinchona Alkaloid-Catalyzed Henry Reaction

Kumpulainen, T.; Qian, J.; Brouwer, A.M.

DOI
10.1021/acsomega.7b01713

Publication date
2018

Document Version
Final published version

Published in
ACS Omega

License
CC BY-NC-ND

Link to publication

Citation for published version (APA):
Kumpulainen, T., Qian, J., & Brouwer, A. M. (2018). Spectroscopic Study of a *Cinchona* Alkaloid-Catalyzed Henry Reaction. *ACS Omega*, *3*(2), 1871-1880. https://doi.org/10.1021/acsomega.7b01713

General rights
It is not permitted to download or to forward/distribute the text or part of it without the consent of the author(s) and/or copyright holder(s), other than for strictly personal, individual use, unless the work is under an open content license (like Creative Commons).

Disclaimer/Complaints regulations
If you believe that digital publication of certain material infringes any of your rights or (privacy) interests, please let the Library know, stating your reasons. In case of a legitimate complaint, the Library will make the material inaccessible and/or remove it from the website. Please Ask the Library: https://uba.uva.nl/en/contact, or a letter to: Library of the University of Amsterdam, Secretariat, P.O. Box 19185, 1000 GD Amsterdam, The Netherlands. You will be contacted as soon as possible.

UvA-DARE is a service provided by the library of the University of Amsterdam (https://dare.uva.nl)

Download date:10 Sep 2026

This is an open access article published under a Creative Commons Non-Commercial No Derivative Works (CC-BY-NC-ND) Attribution License, which permits copying and redistribution of the article, and creation of adaptations, all for non-commercial purposes.

ACS OMEGA

Article

Cite This: ACS Omega 2018, 3, 1871−1880

Spectroscopic Study of a *Cinchona* Alkaloid-Catalyzed Henry Reaction

Tatu Kumpulainen,*[,†] Junhong Qian,[‡] and Albert M. Brouwer*

Van't Hoff Institute for Molecular Sciences, Faculty of Science, University of Amsterdam, P.O. Box 94157, 1090 GD Amsterdam, The Netherlands

Supporting Information

ABSTRACT: A spectroscopic study of an organocatalytic Henry reaction between nitroalkanes and aldehydes catalyzed by a quinidine-derived *Cinchona* alkaloid is described. The binding modes of the reaction substrates are investigated using electronic absorption and fluorescence spectroscopy and further corroborated by nuclear magnetic resonance measurements. Aldehydes are shown to associate with both the 6′-OH group and the basic quinuclidine nitrogen of the catalyst, whereas nitroalkanes do not exhibit a clear binding mode. Reaction progress kinetic analysis reveals that the reaction is first-order in both of the substrates and the catalyst. Second, the reaction proceeds approximately five times faster in the excess of the nitroalkanes than in the excess of the aldehydes, suggesting that binding of the aldehydes results in the inhibition of the catalyst. Aldehydes deactivate the basic quinuclidine site, thus suppressing the deprotonation of the nitroalkanes which is the proposed initial step in the reaction cycle.

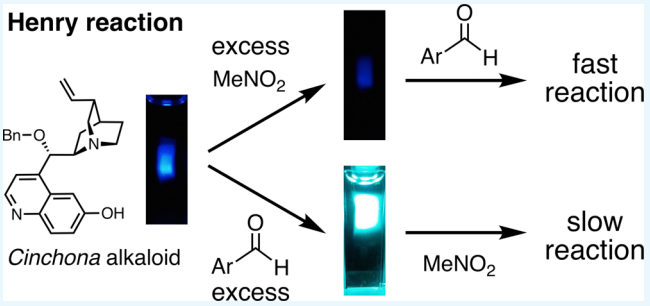

INTRODUCTION

The biological activity of many pharmaceutical compounds, agrochemicals, flavors, and fragrances depends on the absolute stereochemistry of the molecules.[1−3] The growing demand for such chiral molecules has made enantioselective synthesis one of the main goals in organic chemistry during the 21st century.[4] Employment of asymmetric catalysts, such as transition metal complexes or small organic molecules, also known as organocatalysts, represents an effective way toward the synthesis of chiral molecules.[5−9] Transition metal catalysts often suffer from several drawbacks such as high price, toxicity, and sensitivity toward ambient conditions. Asymmetric organocatalysts, on the other hand, offer a "green", metal-free, nontoxic, and low-cost route toward these valuable chemicals and have received increasing attention during the last decades.[10−17]

Among the known organocatalysts, *Cinchona* alkaloid-derived compounds hold a special position and have been used in numerous C−C bond-forming organocatalytic reactions with high yields and enantioselectivities. The *Cinchona* alkaloids are available from natural sources as pairs of pseudoenantiomers, such as quinine and quinidine, which differ only in their absolute configuration at C_8 and C_9. Since the chirality of the catalyst is transferred to the product, the employment of a pseudoenantiomeric pair in asymmetric catalysis gives easy access to both enantiomers of the same product.[15,18−20] The naturally occurring alkaloids contain several functional groups including a basic and nucleophilic quinuclidine, a quinoline unit, a secondary alcohol, and a terminal olefin. The functional richness of the abundant alkaloids allows their conversion to more efficient catalysts with different functionalities[21,22] or immobilization on a support[23−25] in a few synthetic steps.

The catalytic versatility of the *Cinchona* alkaloid catalysts arises from two key factors: conformational flexibility and bifunctionality.[26−28] This was already recognized in the pioneering work of Hiemstra and Wynberg in 1981.[29] The *Cinchona* alkaloids can easily undergo rotations around the C_9−C_8 and the C_9−C_4' bonds (Chart 1) and exist mainly in four different conformations.[26,28] The bifunctionality, on the other hand, is attributed to interactions of the substrates with the basic quinuclidine nitrogen (nucleophile, hydrogen-bond acceptor) and the hydroxyl group (electrophile, hydrogen-bond donor) of the catalyst. The quinuclidine moiety is able to activate a nucleophile, and the hydroxyl group can activate an electrophile or assist in the orientation of the substrates via hydrogen bonding. Despite the large number of mechanistic studies by means of nuclear magnetic resonance (NMR), reaction kinetics, and computational techniques, the understanding of the overall mechanisms of *Cinchona* alkaloid-catalyzed reactions remains limited.[26,27,29−39] In particular, experimental observation of the reaction intermediates is challenging because of the transient and noncovalent nature of the interactions between the catalyst and the substrates.

The functional groups responsible for the catalytic activity can also facilitate different photophysical processes together with the built-in quinoline chromophore. The hydroxy-

Received: November 2, 2017
Accepted: January 5, 2018
Published: February 13, 2018

Downloaded via UNIV AMSTERDAM on May 13, 2019 at 12:46:47 (UTC).
See https://pubs.acs.org/sharingguidelines for options on how to legitimately share published articles.

© 2018 American Chemical Society

DOI: 10.1021/acsomega.7b01713
ACS Omega 2018, 3, 1871−1880

Chart 1. Structures the *Cinchona* Alkaloid Cupreidine-Derived Catalyst and the Model Substrates of the Henry Reaction

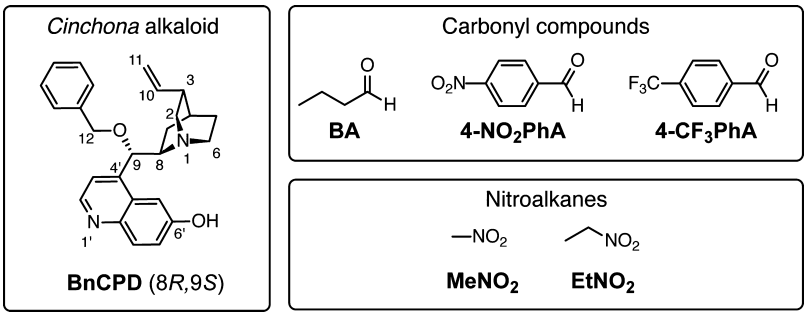

Scheme 1. General Mechanism of the Base-Catalyzed Henry Reaction

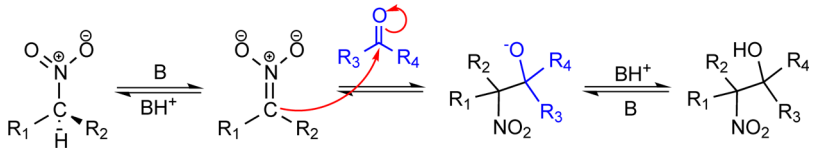

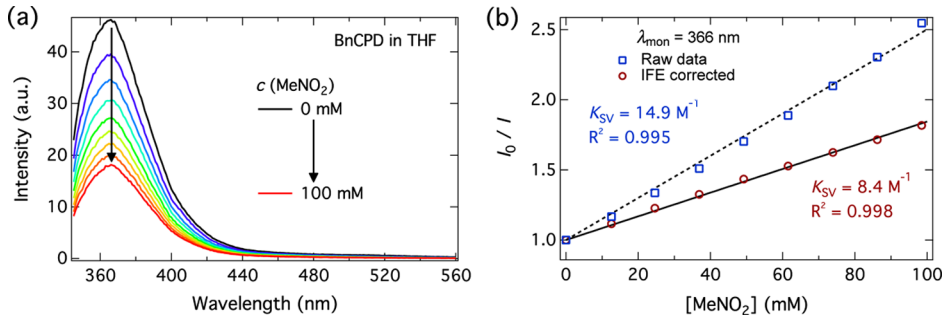

Figure 1. (a) Steady-state emission spectra of **BnCPD** (c = 30 μM) in THF upon addition of **$MeNO_2$**. The spectra are corrected for the primary IFE (see text). The excitation wavelength was 330 nm. (b) Stern–Volmer plots of the uncorrected and primary IFE-corrected emission intensities monitored at 366 nm.

substituted quinoline is an excited-state acid and can undergo intramolecular or intermolecular excited-state proton transfer.[40−42] In addition, the quinuclidine moiety is a good electron donor resulting in quenching of the locally excited (LE) emission of the quinoline and the appearance of a long-wavelength charge-transfer emission band in polar solvents.[43−45] These processes are affected by various hydrogen bonding and protonating agents such as water, acids, bases, and the reaction substrates. Therefore, monitoring of the spectroscopic properties (absorption and emission) potentially enables the observation of weak noncovalent interactions with high sensitivity.

The aim of the present study is to use electronic absorption and emission spectroscopy combined with NMR spectroscopy and reaction progress kinetic analysis to study the binding modes and reaction mechanisms of *Cinchona* alkaloid-derived catalysts. We chose Henry reaction (Scheme 1) as the model reaction.[46−48] The Henry reaction is a base-catalyzed C−C bond-forming reaction between nitroalkanes and aldehydes or ketones. According to the mechanism reported in the literature, the initial step is a deprotonation of the weakly acidic nitroalkane on the α-carbon followed by a nucleophilic attack to the carbonyl-containing substrate to give a potentially chiral β-nitro alkoxide. Protonation of the alkoxide by the protonated base yields the β-nitro alcohol as a product. In *Cinchona* alkaloids and their derivatives, the quinuclidine moiety acts as the base, whereas the hydroxyl group helps to orient the carbonyl compound via hydrogen bonding.[49,50]

The investigated catalyst is the 9-benzyl ether of cupreidine (**BnCPD**),[51] and the model reaction substrates are butyraldehyde (**BA**), 4-nitrobenzaldehyde (**4-NO_2PhA**), and 4-trifluoromethyl-benzaldehyde (**4-CF_3PhA**) as the carbonyl compounds and nitromethane (**$MeNO_2$**) and nitroethane (**$EtNO_2$**) as the nitroalkanes (Chart 1). All measurements are performed in tetrahydrofuran (THF) which is the most used solvent with the current catalyst and reaction.[52] The photophysical properties of **BnCPD** in different solvents, and upon addition of model hydrogen bonding and protonating agents, have been investigated previously in our group.[43,45] Here, we report on a photophysical characterization of **BnCPD** in the presence of model substrates complemented by NMR measurements to study the binding modes of the individual substrates. Second, we present the reaction progress kinetic analysis studies of two model reactions to gain deeper insights into the reaction mechanism.

RESULTS AND DISCUSSION

Binding Mode of the Nitroalkanes. According to the literature, the binding mode of nitroalkanes in the Henry reaction is deprotonation by the basic quinuclidine yielding a contact ion pair which is further stabilized by hydrogen bonding with the hydroxyl group.[50] We have previously shown that the fluorescence decay of **BnCPD** in neat THF exhibits

DOI: 10.1021/acsomega.7b01713
ACS Omega 2018, 3, 1871−1880

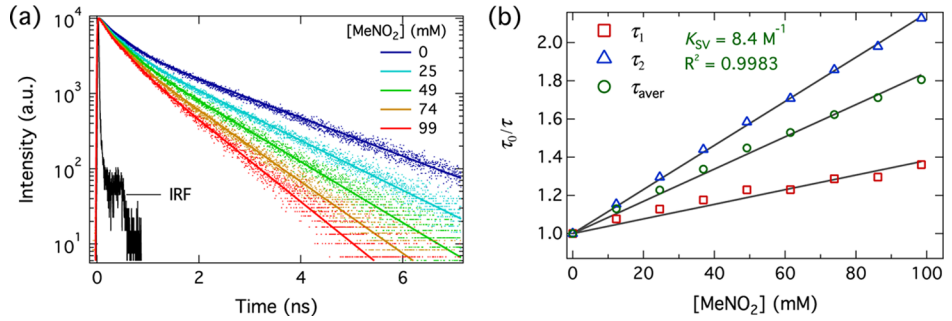

Figure 2. (a) Fluorescence decays of **BnCPD** (c = 30 μM) in THF upon addition of **MeNO$_2$** together with the IRF. The excitation wavelength was 322 nm and the monitoring wavelength was 370 nm. (b) Stern–Volmer plots of the individual lifetimes, τ_1 and τ_2, and the amplitude-weighted average lifetime τ_{aver}. The lifetimes in the absence of **MeNO$_2$** are τ_1 = 0.3 ns, τ_2 = 1.7 ns, and τ_{aver} = 0.8 ns.

two main decay components with time constants of ca. 360 ps and 1.7 ns. The two time constants were attributed to two different conformations of the catalyst, where in one of them, the fluorescence is quenched by either a photoinduced electron-transfer or a proton-transfer process. Moreover, deactivation of the quinuclidine nitrogen by protonation (or hydrogen bonding) suppresses these quenching processes and results in the recovery of the unquenched LE emission.[43,45] Therefore, addition of a nitroalkane is expected to increase the LE emission and suppress the relative amplitude of the quenched component, assuming that the binding mode involves protonation of the quinuclidine nitrogen. Association of the nitroalkane with the quinuclidine is not expected to affect the absorption spectrum of the catalyst in the wavelength range >280 nm.

The steady-state absorption spectrum of **BnCPD** does not exhibit any changes upon the addition of **MeNO$_2$** (Figure S2, Supporting Information). Because of the absorption of **MeNO$_2$** at the excitation wavelength (330 nm), the emission spectra, presented in Figure 1a, were corrected for the primary inner-filter effect (IFE). Contrary to our expectations, the emission intensity decreases upon increasing the concentration of **MeNO$_2$**. Similar fluorescence quenching of anthracene by **MeNO$_2$** has been reported in the literature[53] and was also observed by us in a reference measurement.

We used the Stern–Volmer analysis, as shown in eq 1, to determine the quenching constant from the steady-state emission spectra.

$$\frac{F_0}{F} = 1 + K_{SV}[Q] \tag{1}$$

In the above equation, F_0 and F are the fluorescence intensities in the absence and presence of the quencher (**MeNO$_2$**), K_{SV} is the Stern–Volmer quenching constant, and [Q] is the quencher concentration. The Stern–Volmer plots of the uncorrected and primary IFE-corrected fluorescence data monitored at the maximum (366 nm) are presented in Figure 1b. The Stern–Volmer plot of the uncorrected data exhibits a slight upward curvature, and the determined Stern–Volmer constant is almost two times higher than that for the corrected data. This emphasizes the importance of the IFE correction. The determined Stern–Volmer constant from the corrected spectra is K_{SV} = 8.4 M^{-1}.

The nature of the quenching was investigated by using time-resolved fluorescence. The fluorescence decays of **BnCPD** upon addition of **MeNO$_2$** in THF were measured using the time-correlated single-photon counting (TCSPC) setup and are presented in Figure 2a together with the instrument response function (IRF). The decays were monitored close to the emission maximum at 370 nm. As discussed above, **BnCPD** exhibits two main decay components in neat THF attributed to two different conformations of the molecule.[45] Therefore, the decay curves were analyzed using a biexponential model, and an amplitude-weighted average lifetime, as shown in eq 2, was used for the Stern–Volmer analysis.[54]

$$\tau_{aver} = \sum_{i=1}^{n} \frac{\alpha_i}{\sum \alpha_i} \tau_i \tag{2}$$

In eq 2 α_i is the relative amplitude of the corresponding decay time, τ_i. In the case of pure dynamic (collisional) quenching, the Stern–Volmer equation becomes

$$\frac{F_0}{F} = \frac{\tau_0}{\tau} = 1 + K_D[Q] \tag{3}$$

In the above equation, τ_0 and τ are the average lifetimes in the absence and presence of the quencher and K_D is the dynamic Stern–Volmer quenching constant. The Stern–Volmer plots of the individual lifetimes and the amplitude-weighted average lifetime are presented in Figure 2b. The fit parameters of the individual decays are summarized in Table S1 (Supporting Information).

The Stern–Volmer plot exhibits linear behavior with K_D = 8.4 M^{-1}, determined from the amplitude-weighted average lifetime. The value is identical to that determined from the steady-state measurements. This strongly suggests that the observed changes in the fluorescence intensity can be fully explained by considering dynamic quenching by **MeNO$_2$** without the need to invoke any binding mechanism. However, the relative amplitude of the faster decay component slightly decreases and that of the longer component increases upon the addition of **MeNO$_2$** (see Table S1). This could indicate that a small fraction (<3%) of the catalyst forms a complex with **MeNO$_2$**, which results in the protonation of the quinuclidine nitrogen and generation of longer-lived fluorescent species. The upper limit for the association constant can be estimated to be K_{eq} < 0.30 ± 0.05. Alternatively, the association constant can be estimated from the relative acidities of **MeNO$_2$** ($K_a^{MeNO_2}$) and the protonated quinuclidine nitrogen ($K_a^{QH^+}$) according to $K_{eq} = K_a^{MeNO_2}/K_a^{QH^+}$. The p$K_a$ value of **MeNO$_2$** is 10.2, whereas that of the quinuclidine group in quinine/quinidine-derived *Cinchona* alkaloids is 8.8–9.7.[43,55−57] This results in an association constant of 0.04 < K_{eq} < 0.32, in good agreement with the value estimated above.

DOI: 10.1021/acsomega.7b01713
ACS Omega 2018, 3, 1871−1880

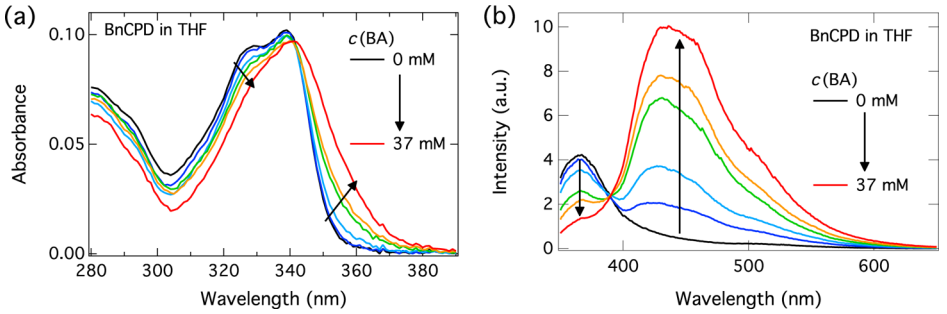

Figure 3. Steady-state (a) absorption and (b) emission spectra of **BnCPD** (c = 20 μM) in THF upon addition of **BA**. Absorption of **BA** has been subtracted from that of the **BnCPD** sample, and the emission spectra are corrected for the primary IFE. The excitation wavelength was 330 nm.

To investigate the binding mode further, we measured proton NMR (^{1}H NMR) spectra of **BnCPD** in the absence and presence of the nitroalkanes, (**MeNO$_2$**) and (**EtNO$_2$**), at concentrations representative for catalytic reactions in THF-d_8. The concentrations of the samples were **BnCPD** (14 mM) + **MeNO$_2$** (140 mM) and **BnCPD** (29 mM) + **EtNO$_2$** (290 mM). The ^{1}H NMR spectra showed only a broadening of the 6′-OH proton signal (δ = 8.97 ppm) of **BnCPD** upon the addition of nitroalkanes (Figure S3, Supporting Information). The broadening can be attributed to dynamic hydrogen-bonding interactions between the nitroalkanes and the catalyst. No shifts in any of the proton signals of the quinuclidine moiety were observed, which means that the concentration of the protonated catalysts is very low. However, assuming the upper limit of K_{eq} < 0.3 as determined above, the concentration of the binary complex would be on the order of the detection limit of NMR measurements (ca. 5%).

Binding Mode of the Aldehydes. The carbonyl compounds, in this case, the aldehydes, are assumed to bind to the catalyst via hydrogen bonding to the quinoline 6′-OH group. This is expected to influence the spectroscopic properties of the catalyst. The absorption and emission spectra of **BnCPD** upon the addition of **BA** are presented in Figure 3. Absorption of **BA** has been subtracted from the total absorption, and the emission spectra have been corrected for the primary IFE.

Addition of **BA** results in clear changes both in the absorption and the emission spectra of the catalyst. The absorption exhibits a broadening and a red shift of the main absorption band originating from the quinoline moiety. The emission spectra exhibit a decrease in the LE emission and an appearance of a long-wavelength emission band with a maximum at ∼430 nm and a shoulder at ∼520 nm. The observed changes are similar to those observed upon addition of a strong base which results in deprotonation of the quinoline 6′-OH group.[45] This strongly suggests that anionic species are formed upon the addition of **BA**.

Substituted aromatic aldehydes have relatively strong absorption in the absorption range of the catalyst. We therefore investigated only unsubstituted benzaldehyde. The absorption and emission spectra of **BnCPD** upon the addition of benzaldehyde are presented in Figure S4 (Supporting Information), and the spectra are corrected as in the case of **BA**. Addition of benzaldehyde results qualitatively in similar changes as the addition of **BA**. This suggests a similar mode of action for both aldehydes. The sensitivity of the catalyst toward the addition of benzaldehyde is, however, lower compared to that of **BA**.

Determination of association constants was not possible for either of the aldehydes. This was due to the poorly reproducible quantitative behavior upon addition of the aldehydes. The observed spectroscopic changes were dependent on the light exposure as demonstrated by control measurements. Continuous monitoring of the long-wavelength emission intensity of a fresh **BnCPD** + **BA** sample at 430 nm showed that the emission intensity increases with time. Moreover, the increase was faster when the sample was excited at the absorption maximum of the aldehyde. Second, a single addition of 33 mM benzaldehyde did not reproduce the changes observed upon the incremental additions. However, the emission showed a gradual increase similar to that presented in Figure 3b when the emission spectra were measured several times after each other without changing the sample nor the experimental conditions. The observed changes were clearly dependent on the light exposure of the sample but, unfortunately, selective excitation of the catalyst was not possible because of the overlap with the aldehyde absorption.

The nature of the long-wavelength emission band was also investigated by using time-resolved fluorescence. The decays were monitored between 360 and 500 nm and fitted globally with a three-exponential model convolved with the measured IRF. The excitation wavelength was 315 nm. The decay-associated spectra (DAS, see Supporting Information) of **BnCPD** in the presence of **BA** are presented in Figure 4.

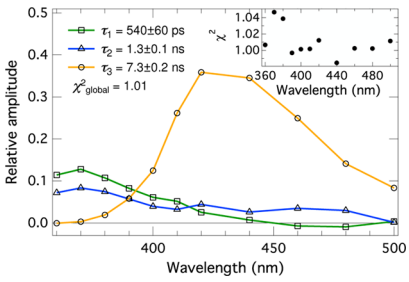

Figure 4. Decay-associated fluorescence spectra of **BnCPD** (c = 40 μM) in the presence of **BA** (c = 15 mM) in THF. The inset shows the individual χ^2-values. The excitation wavelength was 315 nm.

The decays exhibit three main components. The two faster components (τ_1 = 0.54 ns and τ_2 = 1.3 ns), responsible for the LE emission, are similar to those observed for **BnCPD** in neat THF (τ_1 = 0.36 ns and τ_2 = 1.7 ns).[45] Although the lifetimes are slightly different, these components can be attributed to the two conformations of **BnCPD** similar to the case in neat THF. The main component responsible for the red-shifted emission has a significantly longer lifetime (τ_3 = 7.3 ns) characteristic of

DOI: 10.1021/acsomega.7b01713
ACS Omega 2018, 3, 1871−1880

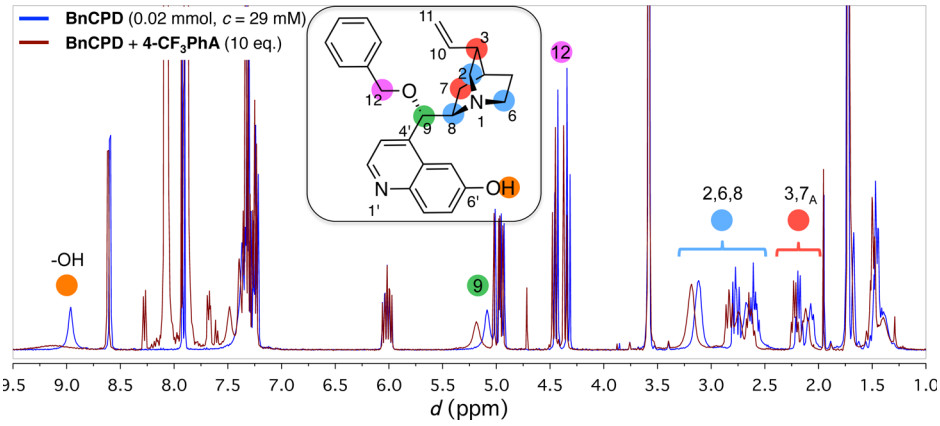

Figure 5. ^{1}H NMR spectra of **BnCPD** (0.02 mmol, c = 29 mM) in the absence (blue) and presence (red) of **4-CF$_3$PhA** (0.2 mmol, c = 290 mM) in THF-d_8. The protons of the catalyst exhibiting significant changes in their chemical shifts are indicated in the figure.

Scheme 2. Proposed Binding Mode of the Aldehydes and the Structure of the Zwitterionic Photoproduct Observed in the UV–Vis Measurements

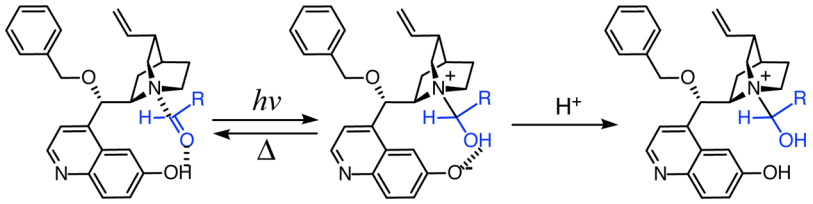

an anionic species. The shorter components do not exhibit significant negative amplitude in the long-wavelength region. This suggests that the long-wavelength-emitting species is formed directly upon the excitation of a ground-state species, not photochemically via a transient state, for example, the LE state of the neutral catalyst. Similar behavior was observed for **BnCPD** in the presence of benzaldehyde (Figure S5, Supporting Information). Although the formation of the anionic species is photochemically irreversible, addition of an acid to the reaction mixture after light exposure resulted in the recovery of the LE emission and disappearance of the long-wavelength emission. The DAS of the **BnCPD/BA** mixture upon addition of an acid are presented in Figure S6. The results demonstrate that 6′-hydroxyquinoline moiety remains intact in the anionic species, and the deprotonation/protonation of the 6′-OH is chemically reversible.

Again, we turned to ^{1}H NMR measurements to study the binding mode of the aldehydes at catalytic concentrations and to avoid the irreversible photochemical reaction. ^{1}H NMR spectra of **BnCPD** were measured in the presence of all three aldehydes. Representative ^{1}H NMR spectra of **BnCPD** in the absence and presence of **4-CF$_3$PhA** are presented in Figure 5. The protons of **BnCPD** exhibiting significant changes in their chemical shifts are indicated in the figure.

Addition of all three aldehydes results in downfield shifts of multiple proton signals of the catalyst. The changes are largest upon the addition of **4-CF$_3$PhA**. The aldehydes exhibit a clear association with the 6′-OH group resulting in a strong broadening and red shift of the proton signal at δ = 8.97 ppm. In addition, the spectra show shifts in the proton signals of the quinuclidine moiety. The shifts are especially clear for the hydrogen that are nearest to the basic quinuclidine nitrogen at δ = 2.5–3.3 ppm (H2, H6, and H8). Interestingly, the H12 protons of the side group also exhibit a small shift. This possibly results from a change in the conformation of the catalyst. Binding of the aldehydes to the catalytic pocket most likely increases the population of a conformation in which the substrate is simultaneously bound to both the 6′-OH and the quinuclidine nitrogen. Wang and co-workers reported similar observations for a thiourea-functionalized *Cinchona* alkaloid.[31] Addition of a single reaction substrate, in their case, the nucleophile, (N-Boc-α,β-unsaturated-γ-butyrolactam) to a solution of the catalyst in C_6D_6 resulted in downfield shifts of most of the catalyst proton signals. This was attributed to an association of the substrate with both the basic quinuclidine and the hydrogen-bond donating thiourea moieties of the catalyst.

The ultraviolet–visible (UV–vis) measurements demonstrated a clear interaction between the catalyst and the aldehydes but the excitation of the complex resulted in the irreversible formation of "anionic" species. ^{1}H NMR measurements supported the complex formation and showed that the aldehydes interact with both the 6′-OH group and the quinuclidine moiety. Possible structures of the complex and the "anionic" photoproduct of **BnCPD** with **BA** are presented in Scheme 2. According to the proposed binding mode, the hydrogen bond of the 6′-OH group to the aldehydes decreases the electron density on the carbonyl carbon, which then associates with the lone pair of the basic quinuclidine nitrogen. This is enabled by the close proximity and favorable orientation of the two functional groups in the active (i.e., anticlosed)[29] conformation of the catalyst. Excitation of this neutral complex results in the proton transfer to the carbonyl oxygen and the formation of a covalent bond between the quinuclidine nitrogen and carbonyl carbon. Addition of an acid to the zwitterionic complex protonates the 6′-O$^-$, recovering the neutral LE emission of the quinoline moiety.

Because we did not observe a clear binding of the nitroalkanes, we consider the possibility that the neutral complex between the aldehyde and the catalyst could be the

DOI: 10.1021/acsomega.7b01713
ACS Omega 2018, 3, 1871–1880

Table 1. Reaction Scheme and the Samples Used for the Kinetic Study of BnCPD-Catalyzed Henry Reaction between $MeNO_2$ and 4-NO_2PhA[a]

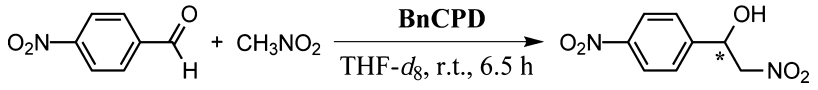

entry	BnCPD (mol %)	$MeNO_2$ (equiv)	4-NO_2PhA (equiv)	conversion[b] (%)
1	10	1	5[c]	79[d]
2	5	10	1	96
3	7.5	10	1	98
4	10	10	1	99
5	12.5	10	1	99

[a]Conditions: 1 equiv = 0.2 mmol, t = 6.5 h, THF-d_8, V = 700 μL, and rt = 22 ± 1 °C. [b]Estimated from the ^{1}H NMR spectra of the reaction mixture. [c]2 mmol of **4-NO_2PhA** was not soluble in 700 μL. Therefore, 1 mmol was used instead. [d]Reaction did not complete within 6.5 h.

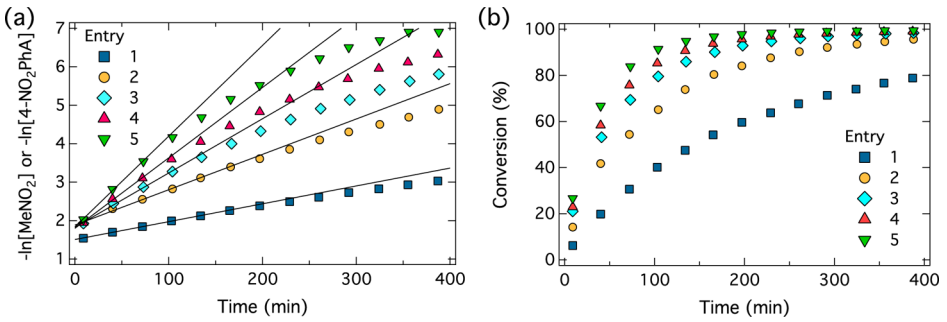

Figure 6. Pseudo-first-order kinetic analysis (a) and calculated conversions (b) of the samples. The slopes of the fitted lines in (a) equal to the observed pseudo-first-order rate constant, k'' (see the Supporting Information). Because of the deviation from the linear trend, we fitted only the beginning of each trace (3−5 data points). The samples and the reaction conditions are listed in Table 1.

initial species in the catalytic cycle contrary to the mechanism proposed in the literature. We explored this possibility by kinetic studies.

Kinetic Studies of the Henry Reaction. We started the kinetic studies by exploring a reaction between **$MeNO_2$** and **4-NO_2PhA** catalyzed by **BnCPD** in THF-d_8. Enantiomeric excesses up to 40% with the *S* absolute configuration of the major enantiomer have been reported for this reaction.[52] The reaction scheme and the samples are presented in Table 1. The aim was to determine the reaction order in each substrate by monitoring the reaction in a large excess of one of the substrates (entries 1 and 4). The order in the catalyst was determined from the relative rate constants at different catalyst loadings (entries 2−5). Second, we wanted to compare the observed rate constant in the excess of the aldehyde to that observed in the excess of the nitroalkane.

The reaction was monitored using ^{1}H NMR spectroscopy. We used an automated sample changer of the spectrometer to monitor all five reactions simultaneously. This limited the data collection of each sample to ∼30 min intervals. Concentrations of the substrates and the product were obtained from the integrals of the proton signals relative to a catalyst signal (used as a standard) and by normalizing it to the known catalyst concentration. The ^{1}H NMR spectra of entries 1 and 4 are shown in Figures S7 and S8, respectively (Supporting Information). We used a pseudo-first-order kinetics method to analyze the data.[58] The initial rate constant, k'', were obtained by linear fitting of the beginning of each trace. The analysis and the calculated conversions of the samples are presented in Figure 6. The observed initial pseudo-first-order rate constants (entries 2−5) as a function of the catalyst loading are presented in Figure 7.

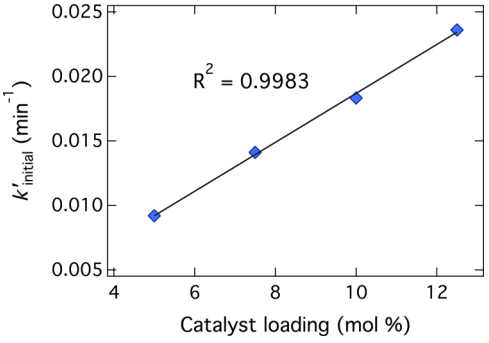

Figure 7. Observed initial pseudo-first-order rate constants of entries 2−5 as a function of the catalyst loading.

The rate constants increase linearly upon increasing the catalyst loading demonstrating that the reaction is first-order in the catalyst (Figure 7). All entries exhibit deviation from the linear trend after reaching ∼60−80% conversion. For entries 4 and 5, the deviation is noticeable already after a few data points because of the slow sampling time relative to the rate of the reaction. This is tentatively attributed to a catalyst inhibition by the product. The hydroxyl group of the product is a better hydrogen-bond donor than the substrates and can block the active site of the catalyst. Because of the inhibition and slow sampling time, we could not unambiguously determine the reaction order in the substrate concentrations. Second, the NMR spectra showed that, in the excess of the aldehyde (entry 1), the primary product reacted with the aldehyde generating a dihydroxy side product which prevented the comparison between the rate constants of entries 1 and 4.

To overcome the problems of the first kinetic study, **$EtNO_2$** and **4-CF_3PhA** were used as the reaction substrates. The

DOI: 10.1021/acsomega.7b01713
ACS Omega 2018, 3, 1871−1880

Table 2. Reaction Scheme and the Samples Used for the Kinetic Study of BnCPD-Catalyzed Henry Reaction between $EtNO_2$ and 4-CF_3PhA[a]

entry	**BnCPD** (mol %)	**$EtNO_2$** (equiv)	**4-CF_3PhA** (equiv)	*t* (min)	conversion (%)
1	20	10	1	300	96
2	20	1	10	430	86

[a]Conditions: 1 equiv = 0.07 mmol, THF-d_8, V = 500 μL, and 40 ± 1 °C.

product of this reaction has a single α-hydrogen next to the nitro group which is expected to suppress the side reaction between the primary product and the aldehyde. In addition, concentrations of the substrates were decreased to half of those in the first study while maintaining the catalyst concentration to increase the accuracy of the relative integration of the NMR signals. This effectively increases the catalyst loading to 20 mol %. To compensate for the decreased reaction rate because of the lower concentration of the substrates (1/2 × 1/2 = 1/4), the temperature was raised to 40 °C. As a rough approximation, increase of ∼20 °C is expected to increase the rate by a factor of four.[59] The reaction progress was monitored using ^{1}H NMR with increasing time intervals (1−20 min). The beginning of the reaction (0−15 min) was not sampled due to setting up of the measurement (locking and shimming) and to stabilize the temperature. We used the reaction progress kinetic analysis method[60] to construct the so-called graphical rate equations (rate as a function of concentration of the substrate not in excess) as described in the Supporting Information. The reaction scheme and the samples are presented in Table 2, and the graphical rate equations of the reactions are presented in Figure 8.

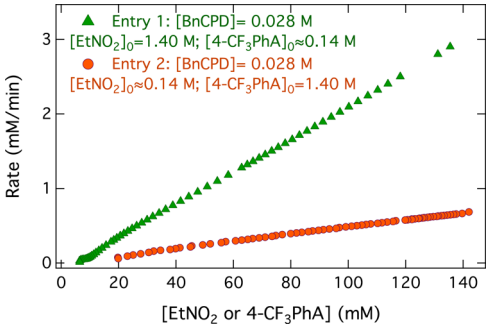

Figure 8. Rate as a function of the minor substrate concentration of **BnCPD**-catalyzed Henry reactions between **$EtNO_2$** and **4-CF_3PhA**. The reaction conditions are listed in Table 2.

The ^{1}H NMR spectra of the entries of Table 2 are shown in Figures S9 and S10, respectively (Supporting Information). Both reactions showed a clean conversion to the desired product as a mixture of two diastereomers. The diastereomeric ratio was dr = 1.3:1 as determined from the ratio of the proton signals. The absolute configuration or the enantiomeric excess of the two diastereomers was not investigated.

The rates of both reactions decrease linearly upon decreasing the substrate concentration. This demonstrates that the reaction is first order in both of the reactants. The slight deviation at the end of the reaction is most likely because of catalyst inhibition by the product. Because of the identical conditions (same overall concentrations and temperature) comparison of the rates is now possible. The reaction performed in the excess of **$EtNO_2$** exhibits approximately five times higher rate than that performed in the excess of **4-CF_3PhA**. This clearly demonstrates that the binding of the aldehyde inhibits the reaction, and the binding mode presented in Scheme 2 does not play a role in the likely reaction pathway. Binding of the aldehyde is additionally observed by comparing the catalyst proton signals between the two reaction mixtures (Figure S11, Supporting Information). Most of the quinuclidine signals exhibit a significant downfield shift in the excess of the aldehyde, similar to that observed in Figure 5. The much higher rate in the excess of **$EtNO_2$** suggests that the initial step is the deprotonation of the nitroalkane by the basic quinuclidine, as proposed in the literature. According to computational studies on related systems, deprotonated nitroalkane forms an ion−pair complex with the protonated quinuclidine, which is stabilized by hydrogen-bonding interactions (Scheme 3). Further on, the aldehyde can form hydrogen bonds to either the protonated quinuclidine or the 6′-OH group to form the reactive tertiary complex. The absolute configuration of the product is determined by a subtle interplay between the hydrogen-bonding interactions between the catalyst and the reaction substrates and the solvent.[30,34,49,61]

CONCLUSIONS

We have used UV−vis and NMR spectroscopies in combination with the reaction kinetic analysis to study the

Scheme 3. Proposed Binding Mode of the Nitroalkanes via Deprotonation by the Basic Quinuclidine Moiety

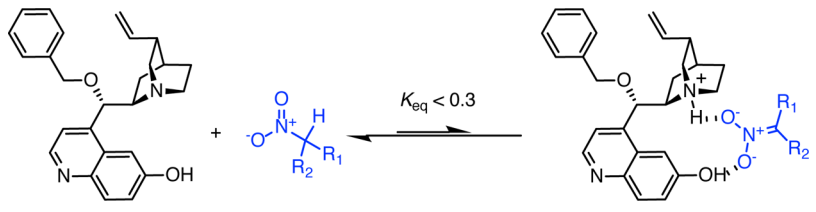

DOI: 10.1021/acsomega.7b01713
ACS Omega 2018, 3, 1871−1880

binding modes and reaction mechanism of an organocatalytic Henry reaction between nitroalkanes and aldehydes. The reaction is catalyzed by the previously studied *Cinchona* alkaloid catalyst **BnCPD**. According to the literature, the reaction proceeds via deprotonation of the nitroalkane by the basic site of the catalyst followed by nucleophilic attack to the aldehyde to form the product.

Addition of nitroalkanes is found to result in the dynamic quenching of the intrinsic fluorescence of the catalyst without clear evidence of complex formation. The NMR measurements show a weak interaction between the hydroxyl group of the catalyst and the nitroalkanes at catalytic concentrations. Aldehydes, on the other hand, exhibit strong interactions with both the hydroxyl group and the quinuclidine moiety of the catalyst as evidenced by both the UV−vis and the NMR measurements. The substrate forms a bridge between the two functional groups of the catalyst. This type of a binding mode changes the conformational distribution of the catalyst toward the closed conformation.

The reaction displays first-order kinetics with respect to the catalyst and the substrates. A slight deviation from the first-order kinetics at high conversions is attributed to a catalyst inhibition by the product. The reaction proceeds approximately five times faster in the excess of the nitroalkane than in the excess of the aldehyde under identical reaction conditions. Therefore, binding of the aldehydes to the active site of the catalyst results in the inhibition of the reaction and does not play a role in the catalytic cycle.

EXPERIMENTAL SECTION

Materials. **BnCPD** was synthesized according to the procedure reported in the literature[51] and subsequently purified twice by recrystallization from ethyl acetate/petroleum ether. **$MeNO_2$** (ReagentPlus, ≥99%), nitroethane (ReagentPlus, ≥99.5%), **BA** (≥99.5%), benzaldehyde (≥99.5%), and 4-(trifluoromethyl)benzaldehyde (98%) were from Sigma-Aldrich. 4-Nitrobenzaldehyde (98%) was from Merck, and THF-d_8 was from Euriso-Top. **BA** and 4-(trifluoromethyl)-benzaldehyde were purified by distillation and stored under nitrogen. Other chemicals were used without further purification. THF was of spectroscopic grade, distilled from sodium and benzophenone, stored over 4 Å molecular sieves, and handled under nitrogen atmosphere.

Spectroscopic Measurements. Steady-state absorption and fluorescence spectra were recorded using a Shimadzu UV-2700 spectrophotometer and a SPEX Fluorolog3-22 fluorimeter, respectively. The fluorescence spectra were collected in a right-angled geometry and corrected for the spectral sensitivity of the instrument. All measurements were carried out at room temperature (21 ± 1 °C) using nondegassed samples. The experimental setup for the measurements of the fluorescence lifetimes (TCSPC) is described in the Supporting Information.

ASSOCIATED CONTENT

Supporting Information

The Supporting Information is available free of charge on the ACS Publications website at DOI: 10.1021/acsomega.7b01713.

Experimental details; data analysis methods; fluorescence decay parameters; and supplementary electronic, decay associated, and ^{1}H NMR spectra (PDF)

AUTHOR INFORMATION

Corresponding Authors

*E-mail: tatu.kumpulainen@unige.ch (T.K.).
*E-mail: a.m.brouwer@uva.nl (A.M.B.).

ORCID

Tatu Kumpulainen: 0000-0001-9469-9294
Albert M. Brouwer: 0000-0002-1731-3869

Present Addresses

†Physical Chemistry Department, Sciences II, University of Geneva, 30, Quai Ernest Ansermet, 1211 Geneva, Switzerland (T.K.).
‡School of Chemistry and Molecular Engineering, East China University of Science and Technology, 200237, Shanghai, China (J.Q.).

Funding

This research was financially supported by the Netherlands Organisation for Scientific Research (NWO).

Notes

The authors declare no competing financial interest.

ACKNOWLEDGMENTS

We thank Prof. Henk Hiemstra for the valuable discussions and careful reading of the manuscript.

REFERENCES

(1) Lahlou, M. Essential oils and fragrance compounds: bioactivity and mechanisms of action. *Flavour Fragrance J.* **2004**, *19*, 159−165.
(2) Caner, H.; Groner, E.; Levy, L.; Agranat, I. Trends in the development of chiral drugs. *Drug Discovery Today* **2004**, *9*, 105−110.
(3) Williams, A. Opportunities for chiral agrochemicals. *Pestic. Sci.* **1996**, *46*, 3−9.
(4) *Chirality in Industry II: Developments in the Commercial Manufacture and Applications of Optically Active Compounds*, 1st ed.; Collins, A. N., Sheldrake, G., Crosby, J., Eds.; John Wiley & Sons Ltd.: West Sussex, 1997.
(5) Knowles, W. S. Asymmetric hydrogenation. *Acc. Chem. Res.* **1983**, *16*, 106−112.
(6) Noyori, R. Asymmetric catalysis: science and opportunities. *Angew. Chem., Int. Ed.* **2002**, *41*, 2008−2022.
(7) Taylor, M. S.; Jacobsen, E. N. Asymmetric catalysis by chiral hydrogen-bond donors. *Angew. Chem., Int. Ed.* **2006**, *45*, 1520−1543.
(8) Ikariya, T.; Murata, K.; Noyori, R. Bifunctional transition metal-based molecular catalysts for asymmetric syntheses. *Org. Biomol. Chem.* **2006**, *4*, 393−406.
(9) Hamilton, G. L.; Kang, E. J.; Mba, M.; Toste, F. D. A powerful chiral counterion strategy for asymmetric transition metal catalysis. *Science* **2007**, *317*, 496−499.
(10) Dalko, P. I.; Moisan, L. In the golden age of organocatalysis. *Angew. Chem., Int. Ed.* **2004**, *43*, 5138−5175.
(11) Pellissier, H. Asymmetric organocatalysis. *Tetrahedron* **2007**, *63*, 9267−9331.
(12) Dondoni, A.; Massi, A. Asymmetric organocatalysis: from infancy to adolescence. *Angew. Chem., Int. Ed.* **2008**, *47*, 4638−4660.
(13) Klier, L.; Tur, F.; Poulsen, P. H.; Jørgensen, K. A. Asymmetric cycloaddition reactions catalysed by diarylprolinol silyl ethers. *Chem. Soc. Rev.* **2017**, *46*, 1080−1102.
(14) Chauhan, P.; Kaya, U.; Enders, D. Advances in organocatalytic 1,6-addition reactions: enantioselective construction of remote stereogenic centers. *Adv. Synth. Catal.* **2017**, *359*, 888−912.
(15) De Bo, G.; Leigh, D. A.; McTernan, C. T.; Wang, S. A complementary pair of enantioselective switchable organocatalysts. *Chem. Sci.* **2017**, *8*, 7077−7081.
(16) Otevrel, J.; Bobal, P. Biphenyl-based bis(thiourea) organocatalyst for asymmetric and *syn*-selective Henry reaction. *Synthesis* **2017**, *49*, 593−603.

DOI: 10.1021/acsomega.7b01713
ACS Omega 2018, 3, 1871−1880

(17) Raeisolsadati Oskouei, M.; Brouwer, A. M. Organocatalytic fluorogenic synthesis of chromenes. *J. Fluoresc.* **2017**, *27*, 1141−1147.
(18) Connon, S. J. Asymmetric catalysis with bifunctional cinchona alkaloid-based urea and thiourea organocatalysts. *Chem. Commun.* **2008**, *0*, 2499−2510.
(19) Marcelli, T.; Hiemstra, H. Cinchona alkaloids in asymmetric organocatalysis. *Synthesis* **2010**, 1229−1279.
(20) Melchiorre, P. Cinchona-based primary amine catalysis in the asymmetric functionalization of carbonyl compounds. *Angew. Chem., Int. Ed.* **2012**, *51*, 9748−9770.
(21) Vakulya, B.; Varga, S.; Csámpai, A.; Soós, T. Highly enantioselective conjugate addition of nitromethane to chalcones using bifunctional Cinchona organocatalysts. *Org. Lett.* **2005**, *7*, 1967−1969.
(22) Marcelli, T.; van Maarseveen, J. H.; Hiemstra, H. Cupreines and Cupreidines: an emerging class of bifunctional Cinchona organocatalysts. *Angew. Chem., Int. Ed.* **2006**, *45*, 7496−7504.
(23) Youk, S. H.; Oh, S. H.; Rho, H. S.; Lee, J. E.; Lee, J. W.; Song, C. E. A polymer-supported Cinchona-based bifunctional sulfonamide catalyst: a highly enantioselective, recyclable heterogeneous organocatalyst. *Chem. Commun.* **2009**, *0*, 2220−2222.
(24) Cancogni, D.; Mandoli, A.; Jumde, R. P.; Pini, D. Silicone-supported Cinchona alkaloid derivatives as insoluble organocatalysts in the enantioselective dimerization of ketenes. *Eur. J. Org. Chem.* **2012**, 1336−1345.
(25) Lee, J.-W.; Mayer-Gall, T.; Opwis, K.; Song, C. E.; Gutmann, J. S.; List, B. Organotextile catalysis. *Science* **2013**, *341*, 1225−1229.
(26) Dijkstra, G. D. H.; Kellogg, R. M.; Wynberg, H.; Svendsen, J. S.; Marko, I.; Sharpless, K. B. Conformational study of Cinchona alkaloids. A combined NMR, molecular mechanics and X-ray approach. *J. Am. Chem. Soc.* **1989**, *111*, 8069−8076.
(27) Cucinotta, C. S.; Kosa, M.; Melchiorre, P.; Cavalli, A.; Gervasio, F. L. Bifunctional catalysis by natural Cinchona alkaloids: a mechanism explained. *Chem.—Eur. J.* **2009**, *15*, 7913−7921.
(28) Nicu, V. P.; Domingos, S. R.; Strudwick, B. H.; Brouwer, A. M.; Buma, W. J. Interplay of exciton coupling and large-amplitude motions in the vibrational circular dichroism spectrum of dehydroquinidine. *Chem.—Eur. J.* **2016**, *22*, 704−715.
(29) Hiemstra, H.; Wynberg, H. Addition of aromatic thiols to conjugated cycloalkenones, catalyzed by chiral β-hydroxy amines. A mechanistic study of homogeneous catalytic asymmetric synthesis. *J. Am. Chem. Soc.* **1981**, *103*, 417−430.
(30) Hammar, P.; Marcelli, T.; Hiemstra, H.; Himo, F. Density functional theory study of the Cinchona thiourea-catalyzed Henry reaction: mechanism and enantioselectivity. *Adv. Synth. Catal.* **2007**, *349*, 2537−2548.
(31) Zhu, J.-L.; Zhang, Y.; Liu, C.; Zheng, A.-M.; Wang, W. Insights into the dual activation mechanism involving bifunctional cinchona alkaloid thiourea organocatalysts: an NMR and DFT study. *J. Org. Chem.* **2012**, *77*, 9813−9825.
(32) Moran, A.; Hamilton, A.; Bo, C.; Melchiorre, P. A mechanistic rationale for the 9-amino(9-deoxy)epi cinchona alkaloids catalyzed asymmetric reactions via iminium ion activation of enones. *J. Am. Chem. Soc.* **2013**, *135*, 9091−9098.
(33) de Freitas Martins, E.; Pliego, J. R., Jr. Unraveling the mechanism of the Cinchoninium ion asymmetric phase-transfer-catalyzed alkylation reaction. *ACS Catal.* **2013**, *3*, 613−616.
(34) Heshmat, M.; Kazaryan, A.; Baerends, E. J. Solvent induced enhancement of enantiomeric excess: a case study of the Henry reaction with cinchona thiourea as the catalyst. *Phys. Chem. Chem. Phys.* **2014**, *16*, 7315−7323.
(35) Lam, Y.-H.; Houk, K. N. Origins of stereoselectivity in intramolecular aldol reactions catalyzed by cinchona amines. *J. Am. Chem. Soc.* **2015**, *137*, 2116−2127.
(36) Grayson, M. N.; Houk, K. N. Cinchona alkaloid-catalyzed asymmetric conjugate additions: the bifunctional Brønsted acid−hydrogen bonding model. *J. Am. Chem. Soc.* **2016**, *138*, 1170−1173.
(37) Martins, E. F.; Pliego, J. R., Jr. A comprehensive theoretical investigation of the transition states and a proposed kinetic model for the cinchoninium ion asymmetric phase-transfer catalyzed alkylation reaction. *J. Mol. Catal. A: Chem.* **2016**, *417*, 192−199.
(38) Lam, Y.-h.; Grayson, M. N.; Holland, M. C.; Simon, A.; Houk, K. N. Theory and modeling of asymmetric catalytic reactions. *Acc. Chem. Res.* **2016**, *49*, 750−762.
(39) Tanriver, G.; Dedeoglu, B.; Catak, S.; Aviyente, V. Computational studies on Cinchona alkaloid-catalyzed asymmetric organic reactions. *Acc. Chem. Res.* **2016**, *49*, 1250−1262.
(40) Bardez, E.; Chatelain, A.; Larrey, B.; Valeur, B. Photoinduced coupled proton and electron transfers. 1. 6-Hydroxyquinoline. *J. Phys. Chem.* **1994**, *98*, 2357−2366.
(41) Bardez, E. Excited-state proton transfer in bifunctional compounds. *Isr. J. Chem.* **1999**, *39*, 319−332.
(42) Mehata, M. S. Photoinduced excited state proton rearrangement of 6-hydroxyquinoline along a hydrogen-bonded acetic acid wire. *Chem. Phys. Lett.* **2007**, *436*, 357−361.
(43) Qin, W.; Vozza, A.; Brouwer, A. M. Photophysical properties of cinchona organocatalysts in organic solvents. *J. Phys. Chem. C* **2009**, *113*, 11790−11795.
(44) Qian, J.; Brouwer, A. M. Excited state proton transfer in the *Cinchona* alkaloid cupreidine. *Phys. Chem. Chem. Phys.* **2010**, *12*, 12562−12569.
(45) Kumpulainen, T.; Brouwer, A. M. Excited-state proton transfer and ion pair formation in a Cinchona organocatalyst. *Phys. Chem. Chem. Phys.* **2012**, *14*, 13019−13026.
(46) Luzzio, F. A. The Henry reaction: recent examples. *Tetrahedron* **2001**, *57*, 915−945.
(47) Palomo, C.; Oiarbide, M.; Laso, A. Recent advances in the catalytic asymmetric nitroaldol (Henry) reaction. *Eur. J. Org. Chem.* **2007**, 2561−2574.
(48) Alvarez-Casao, Y.; Marques-Lopez, E.; Herrera, R. P. Organocatalytic enantioselective Henry reactions. *Symmetry* **2011**, *3*, 220−245.
(49) Li, H.; Wang, B.; Deng, L. Enantioselective nitroaldol reaction of α-ketoesters catalyzed by Cinchona alkaloids. *J. Am. Chem. Soc.* **2006**, *128*, 732−733.
(50) Boruwa, J.; Gogoi, N.; Saikia, P. P.; Barua, N. C. Catalytic asymmetric Henry reaction. *Tetrahedron: Asymmetry* **2006**, *17*, 3315−3326.
(51) Li, H.; Wang, Y.; Tang, L.; Deng, L. Highly enantioselective conjugate addition of malonate and β-ketoester to nitroalkenes: asymmetric C−C bond formation with new bifunctional organic catalysts based on cinchona alkaloids. *J. Am. Chem. Soc.* **2004**, *126*, 9906−9907.
(52) Marcelli, T.; van der Haas, R. N. S.; van Maarseveen, J. H.; Hiemstra, H. Cinchona derivatives as bifunctional organocatalysts for the direct asymmetric nitroaldol (Henry) reaction. *Synlett* **2005**, *18*, 2817−2819.
(53) Ellison, E. H.; Thomas, J. K. Enhanced quenching of anthracene fluorescence by nitroalkanes in zeolite X and Y. *Langmuir* **2001**, *17*, 2446−2454.
(54) Sillen, A.; Engelborghs, Y. The correct use of "average" fluorescence parameters. *Photochem. Photobiol.* **1998**, *67*, 475−486.
(55) Matthews, W. S.; Bares, J. E.; Bartmess, J. E.; Bordwell, F. G.; Cornforth, F. J.; Drucker, G. E.; Margolin, Z.; McCallum, R. J.; McCollum, G. J.; Vanier, N. R. Equilibrium acidities of carbon acids. VI. Establishment of an absolute scale of acidities in dimethyl sulfoxide solution. *J. Am. Chem. Soc.* **1975**, *97*, 7006−7014.
(56) Pedrós, J.; Porcar, I.; Gómez, C. M.; Campos, A.; Abad, C. Interaction of quinine with negatively charged lipid vesicles studied by fluorescence spectroscopy influence of the pH. *Spectrochim. Acta, Part A* **1997**, *53*, 421−431.
(57) Breman, A. C.; van der Heijden, G.; van Maarseveen, J. H.; Ingemann, S.; Hiemstra, H. Synthetic and organocatalytic studies of quinidine analogues with ring-size modifications in the quinuclidine moiety. *Chem.—Eur. J.* **2016**, *22*, 14247−14256.
(58) *Chemical Kinetics: The Study of Reaction Rates in Solution*, 1st ed.; Connors, K. A., Ed.; VCH: New York, 1990.

DOI: 10.1021/acsomega.7b01713
ACS Omega 2018, 3, 1871−1880

(59) *General Chemistry: Principles and Modern Applications*, 10th ed.; Petrucci, R. H., Herring, F. G., Madura, J. D., Bissonnette, C., Eds.; Prentice Hall: New Jersey, 2010.
(60) Blackmond, D. G. Reaction progress kinetic analysis: a powerful methodology for mechanistic studies of complex catalytic reactions. *Angew. Chem., Int. Ed.* **2005**, *44*, 4302−4320.
(61) Marcelli, T.; van der Haas, R. N. S.; van Maarseveen, J. H.; Hiemstra, H. Asymmetric organocatalytic Henry reaction. *Angew. Chem.* **2006**, *118*, 943−945.

DOI: 10.1021/acsomega.7b01713
ACS Omega 2018, 3, 1871−1880